Adaptive Phase Error Suppression Concerning 3D surface Deformation Measurement on Color Digital Fringe Projection Profilometry

Suprijanto [a,*], Naila Zahra [a], Vebi Nadhira [a], Endang Juliastuti [a]

[a] Optics and Image Analysis Laboratory, Instrumentation and Control Research Group, Faculty of Industrial Technology, Institut Teknologi Bandung, Ganesha 10 Bandung, Indonesia,
Corresponding author: *supri@tf.itb.ac.id

Abstract— **3D surface measurement based on phase-shifting profilometry (PSP) has been actively developed in recent years. Three color channels of RGB that are modulated to generate a one-shot PSP method is a concept of color digital fringe pattern profilometry (CDFPP). The CDFPP is a promising technique for the 3D imaging profile of dynamic surface deformation if several phase errors in the one-shot PSP method can be suppressed. This work proposes a processing scheme for phase error suppression schemes (PESS) based on retrieving the modulated sinusoidal fringe and color fringe normalization in PSP using RGB color channel. The processing of PESS consists of tunable bandpass filtering (BPF) followed by fringe normalization. The initial BPF function is defined based on a smoothing spline data set of frequency and power spectrum from the baseline color fringe image. The predefine BPF function could be tunable during the imaging process by considering each frame's condition and RGB channel spectrum mapping. The corrected fringe images are then normalized from the color imbalance, and the phase shift is calculated using the conventional three-step PSP. For evaluation, PESS is performed to reconstruct simulator membrane deformation from four different static profiles and tested to observe the 3D surface of continuous membrane deformation. The PESS could suppress the phase errors of less than 30% less absolute errors than the conventional method and successfully reconstruct the 3D surface for low-frequency continuous membrane deformation with minimizing phase errors.**

Keywords— **Color fringe; profilometry; surface deformation; tunable bandpass filter; smoothing spline.**

I. INTRODUCTION

Non-contact 3D surface measurement is widely used in many applications, such as in quality control inspection, metrology, biometrics, and entertainment. For various non-contact 3D scanner techniques, the optical method based on digital fringe profilometry (DFP) is one of the most researched 3D imaging methods. A typical system configuration uses a digital light processing (DLP) projector and a digital camera with current technology[1], [2].

DFP reconstructs 3D information of a surface based on the phase-modulation and demodulation process. Various methods have been proposed to extract phase information from a DFP measurement. Two of the most common phase demodulation methods are Fourier Transform Profilometry (FTP) [3]–[6] and phase-shifting profilometry (PSP) [7]–[12]. PSP uses *n*-step frames of fringe patterns with different initial phases. PSP is often more preferred due to its robustness in obtaining the modulated phase information. However, for measuring a dynamic deforming surface, conventional PSP would produce a phase shift error due to the object's movement unless the object can be in a static state for at least as long as it takes to project three grayscale fringes onto the object's surface [13]. Regarding this limitation, many researchers have come up with various mathematical compensations for the dynamic application of conventional PSP by solving the problem of motion artifact[6], [14]–[16].

Alternatively, Color Digital Fringe Pattern Profilometry (CDFPP) has been proposed as an alternative for a fast measurement technique and preserving PSP's advantage [17]–[20]. Using CDFPP is possible to apply PSP by only projecting a single frame of a pattern. CDFPP makes use of the idea that a color image consists of three-color channels. Therefore, the three frames greyscale pattern previously used in PSP can be encoded into a single frame of RGB color fringe instead.

Even though the use of color channels in CDFPP seems promising, it does not come without any challenges. The hardware used in DFP, i.e., projector and camera, is intentionally fabricated to have a spectrum overlay and sensitivity to specific colors to accommodate human visual perception [19]–[21]. On the other hand, deliberate fabrication is rather unfortunate for measurement purposes through CDFPP. Several arising problems from the nonlinearity of projector and camera, color coupling, and color imbalance need to be tackled in CDFPP [18], [20]. These problems make image decoupling of a recorded color fringe pattern from each color channel hard to complete correctly and contribute hugely to phase error.

Many approaches have been proposed to solve these drawbacks of color fringe utilization. A scheme based on artificial neural networks (ANN) has been presented as a non-linear mapping to normalize fringe patterns from each color channel [20], [22]. However, an optimal mapping function depends on some strict assumptions about the training process of ANN.

Another proposed solution tends to avoid the color crosstalk problem through rapid sequencing. In the rapid sequencing method, a color CCD camera is substituted by a monochrome CCD camera, and a modified projector is used to minimize the nonlinearity. However, this method requires a fair amount of hardware modification. Besides, it still needs to face greyscale imbalance problems since the monochrome CCD camera might still have different sensitivity for each color[8], [23]. Another method to solve the problem of color images is an iterative process known as several non-linear optimizations. As it is an iterative approach, this scheme has a high computational complexity that is burdensome; it also has a high potential for convergence [5], [18], [24]–[26].

In previous work, Ma et al. [27] proposed a solution to solve the problem in CDFPP, assuming all phase shift errors can be corrected without prior calibration data and on any data model, which is called the blind phase error suppression (BPES). The process consists of a correction to distorted sinusoidal fringes and a color fringe normalization (CFN) to solve the amplitude imbalance of three fringes decoupled from three color channels. However, the method and the bandwidth selection in filtering the fundamental spectrum component (FSC) of the fringe on each color channel image are not systematically described[24], [27]–[29]. Furthermore, there have not been any reports on the method's consideration and application to a dynamic deforming object observation using CDFPP. In fringe normalization, particularly in CDFPP, a selection frequency bandwidth in filtering should consider the phase error due to hardware nonlinearity and a dynamic deforming surface contributing to phase error.

This work proposes a fringe normalization method utilizing a tunable filter that considers the dynamic deforming surface. A tunable bandpass filter (BPF) function is used to optimize a weighting window function, which determines the spatial frequency and spectral power related to the fringe's fundamental spectrum component representing the shape variations of an object's surface observed.

Based on spectrum information from a baseline color fringe, a dataset as a relation between the frequency components in line with the direction of the carrier frequency (f_{cx}) and the power spectrum series with peaks at f_{cx}, is determined. The dataset is used to estimate the predetermined 1D-BPF function using an optimized smoothing spline to find a smoothing factor (λ) in order to minimize phase errors. Furthermore, a 2D function of BPF in each color channel can be numerically obtained by rotating the $H_i(f_x)$ data with respect to zero frequency. The proposed color fringe processing scheme was tested for evaluation by performing continuous 3D surface membrane deformation measurements. The measurement results are then compared with reference data from conventional three-step PSP measurements. This paper is organized as follows. The description of the scheme method is presented in Section 2. The experimental results and discussion of the testing targets are explained in Section 3, and the conclusion is presented in Section 4.

II. MATERIALS AND METHOD

A. The basic Concept of CDFPP

CDFPP is a modification of the three-step phase-shifting profilometry (PSP). The main idea of CDFPP is to encode three sinusoidal fringe images having different initial phases (S_1, S_2, and S_3) into a single color fringe to be projected onto the surface of deforming objects (see Fig. 1).
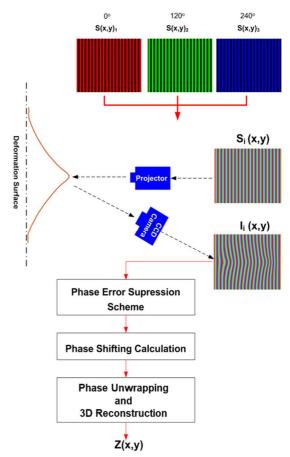

Fig. 1 The Illustration of CDFPP configuration and color fringe processing with the final product of a 3D surface Z(x,y).

By assuming that the fringes have carrier frequency with the orientation in the x-direction, a colored fringe image $S_i(x, y)$ can be modeled as:

$$S_i(x,y) = a_i(x,y) + b_i(x,y)\,cos[f_{cx}x + \alpha_i] \qquad (1)$$

On 1, $i = 1$, 2, and 3 represent the red, green, and blue color channels. An initial phase step is defined by $\alpha_i = 0°, 120°$, $240°$, and f_{cx} is the fringe carrier frequency. Also, a_i and b_i represent the average background intensity and amplitude modulation. For the computer-generated color fringe, a_i and b_i is often set equal for each color channel [27], [30].

When $S_i(x,y)$ is projected onto an object's surface by using the DLP projector, the modulated fringe pattern is recorded by a digital color camera, which can be modeled as

$$I_i(x, y) = a_i(x, y) +$$
$$\sum_{k=1}^{+\infty} b_{k,i}(x, y) \cos[\varphi_i(x, y) + f_{cx}x + \alpha_i] \quad (2)$$

On Eq-2, $b_{k,i}$ is amplitude modulation with harmonic components k [22], [27]. The spectrum mapping of $I_i(x,y)$ can be performed using Fourier Transform (FT) that formulated as

$$FI_i(f_x, f_y) = FT[I_i(x,y)] =$$
$$\sum_N \sum_M I_i(x, y) \cdot exp\left(-j(N.f_x + M.f_y)\right) \quad (3)$$

where f_x, f_y are spatial frequency on x and y direction, respectively, and $N = -(1/2)X$ to $+(1/2)X$ and $M = -(1/2)Y$ to $+(1/2)Y$, where X and Y are the image dimension.
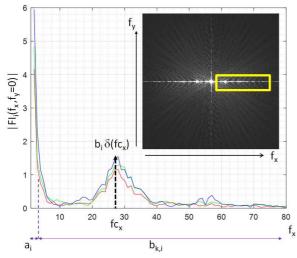

Fig. 2 The Illustration of $|FI_i(f_x, f_y)|$ and $|FI_i(f_x,f_y=0)|$ for range N is marked with the yellow box on the spectral amplitude image ($|FI_i(f_x, f_y)|$). A bandwidth of fundamental spectrum component (FSC) with peak spectral amplitude in fc_x illustrated on plot of $|FI_i(f_x,f_y=0)|$

In this case, $S_i(x,y)$ has f_{cx} with main direction in x-axis, the maximum $|FI_i(f_x, f_y=0)|$ for $f_x \geq 0$ is represented as $b_i\delta(f_{cx})$. Evaluation on the spectral image of $|FI_i(f_x,f_y=0)|$ shown that the fundamental spectrum component (FSC) arise on both lobe-side of $b_i\delta(f_{cx})$ (see Fig. 2). The FCS of $|FI_i(f_x,f_y=0)|$ for $f_x \geq 0$ can be modeled as

$$|FI_i(f_x, f_y = 0)| = a_i + \sum_{N=0}^k b_{N,i} \cdot \delta(f_x N) \quad (4)$$

Based on 4, the parameter $b_{N, i}$ represents a set of FCS harmonic components. The imbalance of the power spectrum of f_{cx} of every color channel could be defined as $b_{n,R}\,\delta(f_{cx}) \neq b_{n,G}\,\delta(f_{cx}) \neq b_{n,B}\,\delta(f_x)$. Furthermore, the distribution of FCS has a specific pattern on each color channel. These problems contribute as a source of phase error in the final 3D reconstruction results. The next section describes the basic concept of phase error suppression scheme.

Phase Error Suppression Scheme (PESS)

As mentioned before, the correction of $I_i(x,y)$ is required to extract the phase shift successfully $\varphi(x,y)$ using the three-step corrected fringe image in each color channel [5], [6]. The basic concept of PESS is summarized in Fig. 3.
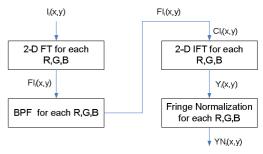

Fig. 3 Basic concept scheme of PESS

The process, performed for all color channels, consists of bandpass filtering followed by fringe normalization. Since the filtered image is used as input for the fringe normalization, the bandpass filter (BPF) on each $I_R(x,y)$, $I_G(x,y)$, and $I_B(x,y)$ is impactful for the error suppression method. The success in suppressing phase error in CDFPP depends on the optimal process both in the BPF design and fringe normalization. In the PESS, a tunable BPF function is proposed to consider each channel's different spatial spectrum characteristics and accommodate the application of CDFPP for a dynamic deforming object.

Tunable BPF function

In the spectrum domain, the filtering process of $I_i(x,y)$ is defined as

$$CY_i(f_x, f_y) = H_i(f_x, f_y) \cdot FI_i(f_x, f_y) \quad (5)$$

where $H_i(f_x, f_y)$ is BPF function, and $i = 1$, 2, 3 represents the R, G, and B channels. As illustrated in Fig.2, the $FI_i(f_x, f_y=0)$ is the spectral data set's main information. Therefore, filter $H_i(f_x, f_y)$ can be designed as 1D-filter $H_i(f_x, f_y=0)$, which will be further denoted by $H_i(f_x)$. Based on its assumption, 5 can be rewritten as

$$CY_i(f_x, f_y = 0) = H_i(f_x) \cdot FI_i(f_x, f_y = 0) \quad (6)$$

Due to the symmetry property of FT, $|CYi(f_x, f_y=0)|$ could be modeled as $|H_i(f_x) \cdot FI(f_x, f_y=0)|$. The role of $H_i(f_x)$ is to select the k-component of FSC and to give weighting factor to the power spectrum of $b_{N,i}\delta(f_{cx})$. However, the bandwidth of FSC centered at $b_{N,i}\delta(f_{cx})$ is always changing in relation to the surface deformation. As illustrated in Fig. 4, the typical bandwidth of FSC obtained from the baseline surface condition (BL) when the membrane is flat and the deforming surface condition (D) in each color channel.

In [27], [31], the $H_i(f_x)$ used is a simple square BPF function, defined as maximum if $\Delta L \leq f_x \leq \Delta H$, with f_{cx} being the center frequency. The illustration of $H_i(f_x)$ is shown in Fig. 5. Using a square function for the $H_i(f_x)$, the power spectral's weighting function around the specific FSC bandwidth highly depends on the definition of ΔL dan ΔH.
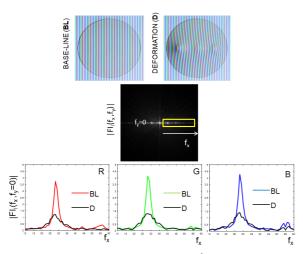
Fig. 4 Illustration of the spectrum range of $\sum_{N>0}^{k} b_{N,i} \cdot \delta(f_{xN})$ on baseline (BL) and deformed (D) condition for each color channel R, G, B.
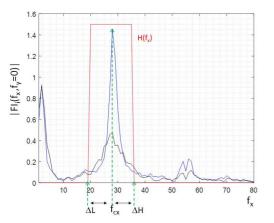

Fig. 5 The illustration of the square function of $H(f_x)$, with $H(f_x)$ uniformly maximum along with the range of $\Delta L \leq f_x \leq \Delta H$ as an effort to give a weight of useful power spectral in the FCS bandwidth for BL (blue line) and D (black line) from the blue channel

In the case of CDFPP, ΔL dan ΔH can be very specific for each color channel and each surface deformation. Therefore, $H_i(f_x)$ should be able to select the FCS bandwidth adaptively. Another feature $H_i(f_x)$ for dynamic CDFPP should be having a proper weighting function for $\sum_{N>0}^{k} b_{N,i} \cdot \delta(f_{xN})$.

The design of the proposed tunable $H_i(f_x)$ starts with analyzing the $\sum_{N>0}^{k} b_{N,i} \cdot \delta(f_{xN})$ of the baseline condition for each color channel ($i = 1, 2, 3$). 1D datasets are defined as $\{f_x, b_{N,i}\delta(f_{xN})\}$ for $\Delta L \leq f_x \leq \Delta H$ including the carrier frequency component $\{f_{cx}, b_{x,i}\delta(f_{cx})\}$. The ΔL is define as minimum value of $b_{N,i}\delta(\Delta L)$ for $\Delta L > 0$ and $\Delta L < f_{cx}$. For $f_x > f_{cx}$, ΔH is defined where $|f_{cx} - \Delta L| = |\Delta H - f_{cx}|$.

Given the data sets $\{f_x, b_{N,i}\delta(f_{xN})\}$ in the range of $\Delta L \leq fx \leq \Delta H$ from the baseline surface condition, an objective smoothing spline function $S_\lambda(\bar{H}_i)$ is minimized to estimate $H_i(f_x)$, which is defined as

$$S_\lambda(\bar{H}_i) = \sum_{j=1}^{n} \left[b_{N,i} \cdot \delta(f_{xN}) - \bar{H}_i(f_{xN}) \right]^2 + \lambda \int \left[\bar{H}_i{''}(f_{xN}) \right]^2 d(f_x) \quad (7)$$

where λ denote a smoothing parameter [32]–[34]. The first term of the objective function $S_\lambda(\bar{H}_i)$ measures the closeness to the data, and the second term penalizes the curvature, which relates to the smoothness. The $\bar{H}_i(f_{xN})$ is estimated based on a

concept of smoothing spline that minimizes $S_\lambda(\bar{H}_i)$ over class of all twice differentiable function on the range of $\{f_{xN}\}$. A smoother curve of the $\bar{H}_i(f_{xN})$ is proportional to the larger value of λ.

The next step is to determine the 2D filter function of $H_i(f_x, f_y)$ based on $H_i(f_x)$ estimation. The 2D filter function is assumed to be a radially symmetric function. The 2D BPF can be numerically obtained by rotating the $\bar{H}_i(f_x)$ data with respect to the distance from its center frequency ($f_X = 0$, $f_X = 0$). After the tunable 2D filter is acquired, it is then applied for the filtering process defined in 5 to obtain $CY_i(f_x, f_y)$ and then followed by inverse FT of $CY_i(f_x, f_y)$ to get the corrected modulated fringe image $Y_i(x,y)$. However, $Y_i(x,y)$ still required fringe normalization to compensate for the imbalance amplitude before the three-step PSI calculation, phase unwrapping, and finally, the $Z(x,y)$ reconstruction to obtain the final output.

B. Fringe Normalization and Final Phase Processing

A fringe normalization is a process to gain back balanced pure sinusoidal forms of the modulated fringe $Y_i(x,y)$ on each color channel. Observation of $Y_i(x,y)$ on the object reference area should show that the amplitude of $Y_R(x,y)$ has the same range as $Y_G(x,y)$ and $Y_B(x,y)$.

For the fringe normalization process, filtered fringe images $CY_i(f_x, f_y)$ (see Fig. 3) is transformed using Hilbert transform $HT(.)$.

$$HT(CY_i(f)) = \delta_H(f) \times CY_i(f) \quad (8)$$

where $f = \{f_x, f_y\}$ and $\delta_H(f)$ is defined as

$$\delta_H(f) = \begin{cases} e^{i\pi/2}, & \text{if } f < 0 \\ 0, & \text{if } f = 0 \\ e^{-i\pi/2}, & \text{if } f > 0 \end{cases} \quad (9)$$

The operator $HT(CY_i(f))$ can be viewed that for negative frequency components of $Y_i(f)$, the phase is shifted for $\pi/2$, and for positive components of $Y_i(f)$ the phase is shifted for -$\pi/2$.

The analytic fringe image $\hat{Y}_i(x, y)$ then can be formulated as

$$\hat{Y}_i(x, y) = Y_i(x, y) + jIFT\{HT(CY_i(f)\} \quad (10)$$

In general, a normalized fringe for each color channel $NY_i(x,y)$ can be written as

$$NY_i(x, y) = \frac{Y_i(x,y)}{\sqrt{Y_i(x,y)^2 + jIFT\{HT(CY_i(f)\}^2}} \quad (11)$$

The result of fringe normalization $NY_i(x,y)$ can be used to determine the wrapped phase $\varphi(x,y)$ through the following formula

$$\varphi(x, y) = tan^{-1}\left(\frac{\sum_{i=1}^{3} NY_i(x,y)\sin(\alpha_i)}{\sum_{i=1}^{3} NY_i(x,y)\cos(\alpha_i)} \right) \quad (12)$$

Then, phase unwrapping is conducted to recover the absolute phase information. Finally, 3D reconstruction, which involves removing the multiple 2π offset, is performed to determine $Z(x,y)$.

C. Procedure for optimization of PESS

The critical process in PESS is the design of tunable $H_i(f_x, f_y)$. After the parameter f_{cx}, ΔL, and ΔH are obtained in

the baseline condition, the smoothing factor λ is yet to be defined. The value of λ is related to a weighting function of estimated H_i (f_x, f_y). Optimized λ value determines the successfulness of the phase error suppression. The value of λ is evaluated iteratively with the objective of finding the optimized value that minimizes the variance (σ^2) of $Z(x,y)$ of the baseline surface condition that defines as

$$\sigma^2 = \frac{I}{NM}\sum(Z(x,y) - \mu) \tag{13}$$

with μ is the mean of $Z(x, y)$. Because $Z(x, y)$ represents the initial surface condition, the optimal λ is related to the smallest σ^2.

D. Experiment Design

The proposed scheme is tested to observe a dynamic deforming membrane surface for evaluation. The membrane simulator is an opaque elastic material. Its membrane is pushed by the arm connected to a controlled DC motor servo. The membrane simulator can be programmed to move continuously with a sinusoidal profile or be maintained in a specific position. The membrane simulator is shown in Fig. 6, and the experiment setup is shown in Fig.7.
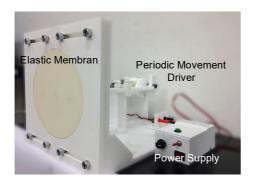

Fig. 6 The membrane simulator observed

As an evaluation for the first experimental setup, the membrane simulator was held in several different positions (A, B, and C), as illustrated in Fig. 8. For the second experiment, a reconstruction of the membrane's continuous movement is observed using the CDFPP. The pusher moves back and forth for continuous movement, pushing the membrane and creating a sinusoidal trajectory.
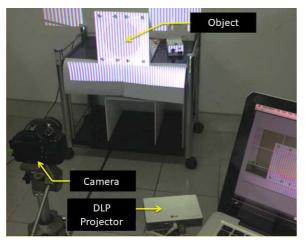

Fig. 7 The experiment setup for CDFPP

III. Results and Discussion

A. Optimization of PESS in Baseline Condition

The baseline condition refers to a flat membrane position or when the pusher is at its minimum point. The baseline condition is used as the reference in defining the optimal value of λ. The iterative process results in defining the optimal λ are shown in Fig 8. The iteration starts with $\lambda=0,01$ and then increases by 0.005 increments. The λ that results in minimum σ^2 of $Z(x,y)$ of the baseline condition is applied for experiments.
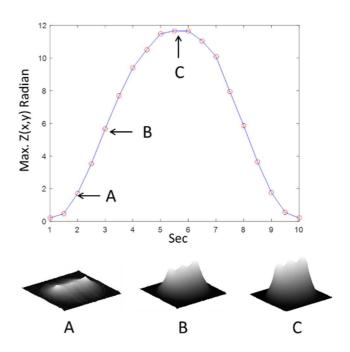

Fig. 8 The profile of membrane simulator. First, the static setup maintains three different membrane positions, $Z(x, y)$ in A, B, and C. The membrane is pushed for a dynamic setup, moving back and forth continuously with a sinusoidal trajectory having a frequency of 1 Hz. The red circle represents the position of the pusher during continuous CDFPP recording.

The example cross-section plot of $Z(x,y)$ on $\lambda=0.01$, 0.03, 0,075 is denoted by A, B, and C, respectively. The reduced value of σ^2 can be seen as related to the value of λ. As shown in Fig. 8, $\lambda = 0.075$ gives the results in the smallest value of σ^2, represented by the red arrow (Top) as well as the red line on the cross-section plot of $Z(x, y)$(Bottom).

B. Evaluation for The First Experiment Setup

The predefined filter design defined from the baseline condition is used for PESS evaluation for continuous 3D measurement of membrane surface deformation. Later the result is compared to reference data from the conventional three-step PSP with gray fringe images with the pusher membrane being maintained in positions A, B, and C (see Fig. 7).

The example of tunable $H_i(f_x)$ and rotated $H_i(f_x)$ into $H_i(f_x, f_y)$ where i = R,G, and B, for the membrane position A and C are shown in Fig. 9. The weighting function of $H_i(f_x)$ in each color channel and two different membrane positions is also presented in Fig. 10.
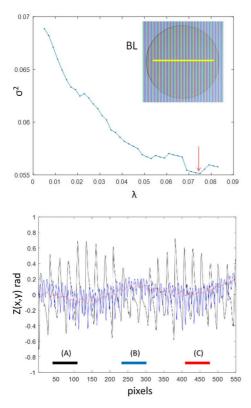
Fig. 9 (Top). Iteration process to determine optimal λ. The red arrow represents the optimal λ resulting in the lowest σ^2. (Bottom) Cross-section plot of the yellow line in the baseline condition, for the definition of $H_i(f_x, f_y)$ with $\lambda=0.01$(**A**), $\lambda=0.03$(**B**), and $\lambda=0.075$(**C**).

The comparison of *the Z(x, y) cross-section in position B* reconstructed using conventional three-step greyscale PSP and CDFPP is presented in Fig.11. The plotted $Z(x, y)$ is the *x*-direction plot of the surface center. The results show the reconstruction using CDFPP (I). Without PESS, (II). With non-tunable $H_i(f_x, f_y)$ PESS, and (III) with tunable $H_i(f_x, f_y)$ PESS. Reduction of σ^2 can be seen in Fig. 10, while the absolute errors between different reconstruction methods using CDFPP of $Z(x,y)$, compared to static greyscale PSP, are tabulated in Table 1.
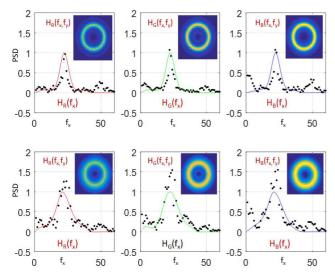

Fig. 10 Tunable $H_i(f_x)$ and rotated $H_i(f_x)$ into $H_i(f_x, f_y)$ where i = R,G and B, for the membrane position A (top row) and C (bottom row)

Surface Position	I Without PESS	II PESS with non-tunable $H_i(f_x, f_y)$	III PESS with tunable $H_i(f_x, f_y)$
A	0.4262	0.0956	0.0022
B	0.5946	0.1985	0.0044
C	0.7324	0.6603	0.0052

C. Evaluation for The Dynamic Observation

The dynamic color fringe images recording of several positions of the membrane, from the baseline position (marked with (1)) to maximum surface amplitude (marked with (8)) shown in Fig 11. The images are obtained from the video recording of continuous deformation of the observed membrane.
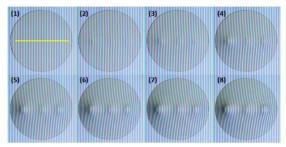

Fig. 11 The color fringe images for continuous surface deformation on eight different pusher positions.

The cross-section plot of $Z(x,y)$ processed using PESS with non-tunable $H_i(f_x, f_y)$ and PESS with tunable $H_i(f_x, f_y)$ are observed to see the reconstruction quality. From Fig. 13, the smoothness of the surface between non-tunable and tunable BPF filter on the PESS is clearly shown.
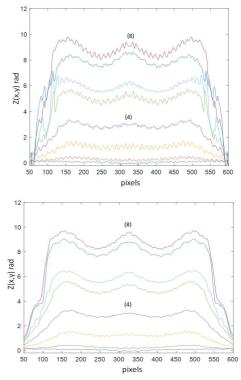

Fig. 13 The plot of $Z(x,y)$ was processed using PESS with non-tunable $H_i(f_x, f_y)$ (left) and PESS with tunable $H_i(f_x, f_y)$ (right) from the color fringe images in Fig. 12.

1978

IV. Conclusion

An alternative scheme of phase error suppression for color digital fringe pattern profilometry concerning continuous surface deformation was developed. The alternative scheme's primary sub-process is a tunable bandpass filter on the spectrum map of color fringe. The tunable BPF is determined based on the 1D-BPF function using an optimized smoothing spline to find a smoothing factor (λ) in order to minimize phase errors. Furthermore, a 2D function of BPF in each color channel can be numerically obtained by the rotation of 1D-BPF function concerning its zero frequency. The predefine BPF function could be tunable during the imaging process by considering each frame's condition and RGB channel spectrum mapping. The corrected fringe images are then normalized from the color imbalance, and the phase shift is calculated using the conventional three-step PSP.

The proposed scheme's performance was also demonstrated by reconstructing the surface profile of a simulator membrane at four different static levels and observing its deformation in a dynamic setting. From the observation, the proposed scheme can suppress the phase errors up to 30% less the absolute errors than the conventional method and successfully reconstruct the 3D surface for low-frequency continuous membrane deformation with minimized phase errors. The method's performance for surface measurement under real vibration or higher frequency needs to be further investigated. Additionally, observation and measurement of colored objects need to be explored.

References

[1] S. Zhang, "Recent progresses on real-time 3D shape measurement using digital fringe projection techniques," *Optics and Lasers in Engineering*, vol. 48, no. 2, pp. 149–158, Feb. 2010, doi: 10.1016/j.optlaseng.2009.03.008.

[2] J. Xu and S. Zhang, "Status, challenges, and future perspectives of fringe projection profilometry," *Optics and Lasers in Engineering*. Elsevier Ltd, p. 106193, Jun. 04, 2020, doi: 10.1016/j.optlaseng.2020.106193.

[3] B. Li, Y. An, and S. Zhang, "Single-shot absolute 3D shape measurement with Fourier transform profilometry," *Applied Optics*, vol. 55, no. 19, p. 5219, 2016, doi: 10.1364/AO.55.005219.

[4] M. Takeda, H. Ina, and S. Kobayashi, "Fourier-Transform Method of Fringe-Pattern Analysis for Computer-Based Topography and Inteferometry.," *Journal of the Optical Society of America*, vol. 72, no. 1, pp. 156–160, 1982, doi: 10.1364/JOSA.72.000156.

[5] M. Padilla, M. Servin, and G. Garnica, "Fourier analysis of RGB fringe-projection profilometry and robust phase-demodulation methods against crosstalk distortion," *Optics Express*, vol. 24, no. 14, p. 15417, 2016, doi: 10.1364/oe.24.015417.

[6] B. Li, Z. Liu, and S. Zhang, "Motion-induced error reduction by combining Fourier transform profilometry with phase-shifting profilometry," *Optics Express*, vol. 24, no. 20, p. 23289, 2016, doi: 10.1364/oe.24.023289.

[7] F. Lü, S. Xing, and H. Guo, "Self-correction of projector nonlinearity in phase-shifting fringe projection profilometry," *Applied Optics*, vol. 56, no. 25, p. 7204, 2017, doi: 10.1364/AO.56.007204.

[8] L. Zhu, Y. Cao, D. He, and C. Chen, "Grayscale imbalance correction in real-time phase measuring profilometry," *Optics Communications*, vol. 376, pp. 72–80, 2016, doi: 10.1016/j.optcom.2016.05.013.

[9] M. Padilla, M. Servin, and G. Garnica, "Profilometry with digital fringe-projection at the spatial and temporal Nyquist frequencies," *Opt. Express*, vol. 25, no. 19, pp. 22292–22302, 2017, doi: 10.1364/OE.25.022292.

[10] S. Xing and H. Guo, "Directly recognizing and removing the projector nonlinearity errors from a phase map in phase-shifting fringe projection profilometry," *Optics Communications*, vol. 435, pp. 212–220, Mar. 2019, doi: 10.1016/j.optcom.2018.11.045.

[11] C. Jiang, S. Xing, and H. Guo, "Fringe harmonics elimination in multi-frequency phase-shifting fringe projection profilometry," *Optics Express*, vol. 28, no. 3, p. 2838, 2020, doi: 10.1364/oe.384155.

[12] C. Y. Liu and C. Y. Wang, "Investigation of Phase Pattern Modulation for Digital Fringe Projection Profilometry," *Measurement Science Review*, vol. 20, no. 1, pp. 43–49, 2020, doi: 10.2478/msr-2020-0006.

[13] M. Duan, Y. Jin, C. Xu, X. Xu, C. Zhu, and E. Chen, "Phase-shifting profilometry for the robust 3-D shape measurement of moving objects," *Optics Express*, vol. 27, no. 16, p. 22100, Aug. 2019, doi: 10.1364/oe.27.022100.

[14] Z. Liu, P. C. Zibley, and S. Zhang, "Motion-induced error compensation for phase shifting profilometry," *Optics Express*, vol. 26, no. 10, p. 12632, 2018, doi: 10.1364/oe.26.012632.

[15] X. Liu, T. Tao, Y. Wan, and J. Kofman, "Real-time motion-induced-error compensation in 3D surface-shape measurement," *Optics Express*, vol. 27, no. 18, p. 25265, 2019, doi: 10.1364/oe.27.025265.

[16] J. Qian, T. Tao, S. Feng, Q. Chen, and C. Zuo, "Motion-artifact-free dynamic 3D shape measurement with hybrid Fourier-transform phase-shifting profilometry," *Optics Express*, vol. 27, no. 3, p. 2713, Feb. 2019, doi: 10.1364/OE.27.002713.

[17] W.-H. Su, "Color-encoded fringe projection for 3D shape measurements," *Optics Express*, vol. 15, no. 20, p. 13167, Oct. 2007, doi: 10.1364/oe.15.013167.

[18] J. Pan, P. S. Huang, and F.-P. Chiang, "Color-encoded digital fringe projection technique for high-speed 3D shape measurement: color coupling and imbalance compensation," *Two- and Three-Dimensional Vision Systems for Inspection, Control, and Metrology*, vol. 5265, no. 1, pp. 205–212, 2004, doi: 10.1117/12.527760.

[19] Y. Hu, J. Xi, J. Chicharo, and Z. Yang, "Blind color isolation for color-channel based fringe pattern profilometry using digital projection," *Journal of the Optical Society of America A*, vol. 24, no. 8, p. 2372, Aug. 2007, doi: 10.1364/josaa.24.002372.

[20] L. Rao and F. Da, "Neural network based color decoupling technique for color fringe profilometry," *Optics and Laser Technology*, vol. 70, pp. 17–25, 2015, doi: 10.1016/j.optlastec.2015.01.007.

[21] W. Li and S. Duan, "Color calibration and correction applying linear interpolation technique for color fringe projection system," *Optik*, vol. 127, no. 4, pp. 2074–2082, 2016, doi: 10.1016/j.ijleo.2015.11.093.

[22] M. J. Baker, J. Xi, and J. F. Chicharo, "Neural network digital fringe calibration technique for structured light profilometers," *Applied Optics*, vol. 46, no. 8, p. 1233, Mar. 2007, doi: 10.1364/AO.46.001233.

[23] M. Ma, Y. Cao, D. He, C. Chen, and Y. Wan, "Grayscale imbalance correcting method based on fringe normalization in RGB tricolor real-time three-dimensional measurement," *Optical Engineering*, vol. 55, no. 3, p. 034102, 2016, doi: 10.1117/1.OE.55.3.034102.

[24] T. T. Chung, T. W. Liu, M. H. Shih, and Y. T. Tu, "Design of color fringe projection sequences for 3D shape measurements," *2010 Symposium on Photonics and Optoelectronic, SOPO 2010 - Proceedings*, pp. 1–4, 2010, doi: 10.1109/SOPO.2010.5504210.

[25] J. L. Flores, A. Muñoz, S. Ordoñes, G. Garcia-Torales, and J. A. Ferrari, "Color-fringe pattern profilometry using an efficient iterative algorithm," *Optics Communications*, vol. 391, no. December 2016, pp. 88–93, 2017, doi: 10.1016/j.optcom.2016.12.058.

[26] C. Jiang et al., "Multi-frequency color-marked fringe projection profilometry for fast 3D shape measurement of complex objects," *Optics Express*, vol. 23, no. 19, p. 24152, 2015, doi: 10.1364/oe.23.024152.

[27] S. Ma, R. Zhu, C. Quan, B. Li, C. J. Tay, and L. Chen, "Blind phase error suppression for color-encoded digital fringe projection profilometry," *Optics Communications*, vol. 285, no. 7, pp. 1662–1668, Apr. 2012, doi: 10.1016/j.optcom.2011.12.027.

[28] K. G. Larkin, D. J. Bone, and M. A. Oldfield, "Natural demodulation of two-dimensional fringe patterns II Stationary phase analysis of the spiral phase quadrature transform," *Journal of the Optical Society of America A*, vol. 18, no. 8, p. 1871, 2001, doi: 10.1364/josaa.18.001871.

[29] J. A. Quiroga and M. Servin, "Isotropic n-dimensional fringe pattern normalization," *Optics Communications*, vol. 224, no. 4–6, pp. 221–227, Sep. 2003, doi: 10.1016/j.optcom.2003.07.014.

[30] Y. Wang, L. Liu, J. Wu, X. Chen, and Y. Wang, "Hilbert transform-based crosstalk compensation for color fringe projection profilometry,"

Optics Letters, vol. 45, no. 8, p. 2199, Apr. 2020, doi: 10.1364/ol.392061.

[31] C. Quan, C. J. Tay, and L. J. Chen, "A study on carrier-removal techniques in fringe projection profilometry," *Optics and Laser Technology*, vol. 39, no. 6, pp. 1155–1161, Sep. 2007, doi: 10.1016/j.optlastec.2006.09.003.

[32] L. Xu and J. Zhou, "A model-averaging approach for smoothing spline regression," *Communications in Statistics: Simulation and Computation*, vol. 48, no. 8, pp. 2438–2451, 2019, doi: 10.1080/03610918.2018.1457694.

[33] D. S. G. Pollock, "Smoothing with Cubic Splines," in *A Handbook of Time Series Analysis, Signal Processing, and Dynamics*, London: Academic Press, 1999, p. 293.

[34] P. Cerejeiras and U. Kähler, "Monogenic Signal Theory," in *Operator Theory*, Springer Basel, 2014, pp. 1–22.